Microstructure and particle-laden flow in diesel particulate filter

Kazuhiro Yamamoto *, Shingo Satake, Hiroshi Yamashita

Department of Mechanical Science and Engineering, Nagoya University, Furo-cho, Chikusa-ku, Nagoya, Aichi 464-8603, Japan

Abstract

Due to the public awareness with regard to harmful diesel emissions, more strict diesel emissions standards such as Euro V in 2008 are being set in the world. As one of the key technologies, a diesel particulate filter (DPF) has been developed to reduce particulate matters (PM) in the after-treatment of exhaust gas. Since the structure of the filter is small and complex, it is impossible to examine the phenomena inside the filter experimentally. In this study, we conducted fluid simulation in DPF. We used the lattice Boltzmann method (LBM). The microstructure of DPF was taken into account. The complex flow pattern appears by using the non-slip boundary condition on the filter wall surface. The soot accumulation was simulated to consider the PM trap in the diesel filter. Results show that the flow is largely changed due to soot deposition. As the soot concentration inside the filter is increased, the filter backpressure is increased.
© 2008 Elsevier Masson SAS. All rights reserved.

Keywords: Diesel particulate filter; Soot; Porous media; Lattice Boltzmann method; Multiphase flow; Darcy's law; Porosity

1. Introduction

Although diesel engines have an advantage of lower fuel consumption in comparison with gasoline engines, diesel exhaust gas has more ambient air pollutants such as NOx and particulate matters (PM) including soot [1]. These emissions are of concern for detrimental effects to human health and the environment, which contribute smog, acid rain, and global warming. Due to the public awareness with regard to harmful emissions, more strict exhaust emissions standards such as Euro V in 2008 are being set in the world.

As one of the key technologies, a diesel particulate filter (DPF) has been developed to reduce PM in the after-treatment of exhaust gas. In simple explanation of DPF, it traps the particles when exhaust gas passes its porous structure. The filtration efficiency is more than 90%. Although some sort of clogging always occurs due to the particle trap, the consequent rise in backpressure could increase fuel consumption and reduce available torque. To develop the filter with lower backpressure and find optimal operation conditions, it is necessary to understand particle accumulation precisely.

So far, the filter has been developed by experiments, and there may not be enough information to investigate the phenomena inside the diesel filter. For better design of DPF with efficiency and durability, it is better to conduct flow simulation with particle in the filter. However, in conventional computational code, it is very challenging to deal with this process, because we need to consider the boundary conditions with complex filter-wall geometry. As an alternative approach, we have focused on the lattice Boltzmann method (LBM).

In LBM, the treatment of boundary conditions is simple and easy, and it is appropriate to calculate porous media flow [2–8]. In our previous studies, we have conducted the flow simulation with soot particles by LBM [9,10]. The particle deposition has been well observed to discuss the flow field and pressure drop inside the porous media. For the filter regeneration process, the soot combustion has been also simulated to discuss the local heat and mass transfer [11,12].

In this study, to examine the flow inside the diesel filter, the real size and geometry of commercialized DPF products are considered. The inner pore structure is formed by simulation of two-phase flow based on our previous approach [9,10]. Then, the flow with soot accumulation is simulated for the PM trap inside the filter.

* Corresponding author. Tel.: +81 52 789 4471; fax: +81 52 789 4471.
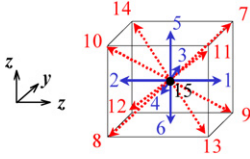*E-mail address:* kazuhiro@mech.nagoya-u.ac.jp (K. Yamamoto).

Fig. 1. D3Q15 model for 3D simulation.

2. Numerical method

We conduct lattice Boltzmann simulation of particle-laden flow in the diesel filter. The fundamental idea of LBM is to construct simplified kinetic models that incorporate the essential physics of microscopic or mesoscopic processes so that the macroscopic averaged properties obey the desired macroscopic equations such as mass and momentum equations [13]. Here, we explain the numerical procedure in simulation. The flow is described by the lattice BGK equation in terms of the velocity distribution function. For three-dimensional simulation, D3Q15 model [10,11,14] evolves on the lattice space with 15 discrete velocities in Fig. 1. The following 15 unit velocity vectors are shown in Eq. (1).

$$
\begin{bmatrix} c_1 & c_2 & c_3 & c_4 & c_5 & c_6 & c_7 & c_8 & c_9 & c_{10} & c_{11} & c_{12} & c_{13} & c_{14} & c_{15} \end{bmatrix}
$$
$$
= c \begin{bmatrix} 1 & -1 & 0 & 0 & 0 & 0 & 1 & -1 & 1 & -1 & 1 & -1 & 1 & -1 & 0 \\ 0 & 0 & 1 & -1 & 0 & 0 & 1 & -1 & 1 & -1 & -1 & 1 & -1 & 1 & 0 \\ 0 & 0 & 0 & 0 & 1 & -1 & 1 & -1 & -1 & 1 & 1 & -1 & -1 & 1 & 0 \end{bmatrix} \tag{1}
$$

To reduce the calculation time, D2Q9 model for 2D simulation is also used to consider the real size of DPF. In the incompressible model, the evolution equation for the distribution function is

$$
p_\alpha(\boldsymbol{x} + \boldsymbol{c}_\alpha \delta_t, t + \delta_t) - p_\alpha(\boldsymbol{x}, t)
$$
$$
= -\frac{1}{\tau}\big[p_\alpha(\boldsymbol{x},t) - p_\alpha^{\text{eq}}(\boldsymbol{x},t)\big] \tag{2}
$$

where δ_t is the time step, and τ is the relaxation time that controls the rate of approach to equilibrium. The equilibrium distribution function, p_α^{eq}, is given by

$$
p_\alpha^{\text{eq}} = w_\alpha \left\{ p + p_0 \left[3\frac{(\boldsymbol{c}_\alpha \cdot \boldsymbol{u})}{c^2} + \frac{9}{2}\frac{(\boldsymbol{c}_\alpha \cdot \boldsymbol{u})^2}{c^4} - \frac{3}{2}\frac{\boldsymbol{u} \cdot \boldsymbol{u}}{c^2} \right] \right\} \tag{3}
$$

where $w_\alpha = 1/9$ ($\alpha = 1$ to 6), $w_\alpha = 1/72$ ($\alpha = 7$ to 14), and $w_{15} = 2/9$, and p_0 is the atmospheric pressure. Also, $c = \delta_x/\delta_t$, where δ_x is the lattice constant. The pressure and local velocity of $\boldsymbol{u} = (u_x, u_y, u_z)$ are obtained by the following two equations.

$$
p = \sum_\alpha p_\alpha \tag{4}
$$

$$
\boldsymbol{u} = \frac{1}{p_0} \sum_\alpha \boldsymbol{c}_\alpha p_\alpha \tag{5}
$$

Through the Chapman–Enskog procedure, the Navier–Stokes equations are derived from these equations [13]. The relaxation time is related with kinetic viscosity as

$$
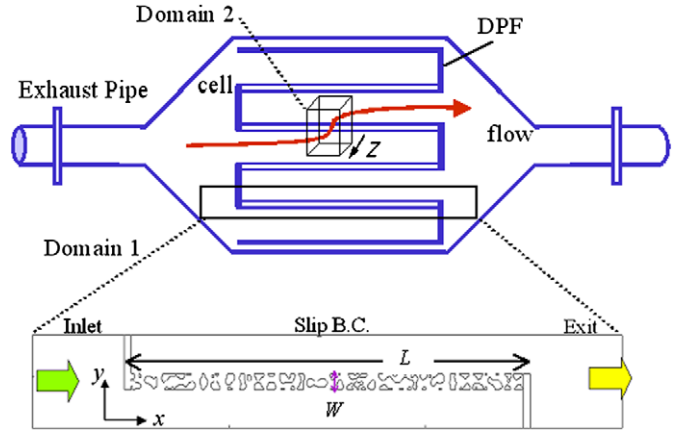\nu = \frac{2\tau - 1}{6} \frac{\delta_x^2}{\delta_t} \tag{6}
$$

Fig. 2. Schematics of DPF system and calculation domain with coordinate.

On the other hand, the soot transport model is based on the so-called passive scalar approach [9,10]. Different from Lagrangian approach through the equation of motion [8], individual particles are not considered. Instead, the soot concentration is monitored at the surface of filter or deposited soot layer. As the soot deposition is continued, the soot concentration at the surface of filter or deposited soot layer sometime becomes unity. When this limit is reached, the solid site is piled up. The deposited soot region is treated as non-slip wall, which implies a dynamically change of boundary condition for flow.

The LB equation for soot mass fraction is,

$$
F_{C,\alpha}(\boldsymbol{x} + \boldsymbol{c}_\alpha \delta_t, t + \delta_t) - F_{C,\alpha}(\boldsymbol{x}, t)
$$
$$
= -\frac{1}{\tau_C}\big[F_{C,\alpha}(\boldsymbol{x},t) - F_{C,\alpha}^{\text{eq}}(\boldsymbol{x},t)\big] + w_\alpha Q_C \tag{7}
$$

where F_C is the distribution function for soot mass fraction, and τ_C is the relaxation time determined by diffusion coefficient. The source term, Q_C, is used so that F_C becomes zero after soot in the gas phase accumulates around the filter wall surface. The equilibrium distribution function, $F_{C,\alpha}^{\text{eq}}$, is given by

$$
F_{C,\alpha}^{\text{eq}} = w_\alpha Y_C \left\{ 1 + 3\frac{(\boldsymbol{c}_\alpha \cdot \boldsymbol{u})}{c^2} + \frac{9}{2}\frac{(\boldsymbol{c}_\alpha \cdot \boldsymbol{u})^2}{c^4} - \frac{3}{2}\frac{\boldsymbol{u}^2}{c^2} \right\} \tag{8}
$$

The mass fraction of soot, Y_C, is obtained in terms of the distribution function by

$$
Y_C = \sum_\alpha F_{C,\alpha} \tag{9}
$$

Fig. 2 shows the schematics of DPF system. This wall-flow filter is mostly designed with a honeycomb structure with adjacent air holes closed at alternate ends so that the exhaust gas passes through the porous filter wall for PM trap. As seen in this figure, two types of calculation domain are adopted. Domain 1 is of 140 mm × 2 mm to simulate the flow in the whole size of one monolith of a cellular filter. The total number of grids is 4201 (N_x) × 61 (N_y). The properties of the filters are shown in Table 1. The monolith length of the cell is L, and the wall thickness is W. The cell concentration is 200 cells/in^2. To consider the different porous structure, we change the mean pore size, d. In this study, the pore sizes are set to be 9 and 33 μm,

Table 1
Properties of DPF in this study

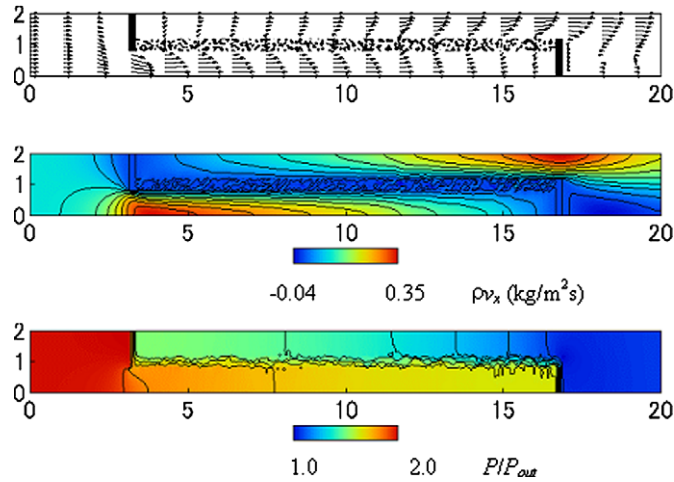| Property	Size
Length, L (mm)	13, 133
Cell size (mm)	1.5×1.5 (200 cells/in^2)
Wall thickness, W (mm)	0.4, 0.6
Porosity, e (%)	42, 60
Mean pore size, d (μm)	9, 20, 33

Fig. 3. Velocity field in DPF for $e = 0.6$, $L = 13$ mm, $d = 33$ μm, $U_0 = 10$ cm/s; velocity vector, mass flux in x-direction, and pressure distributions are shown.
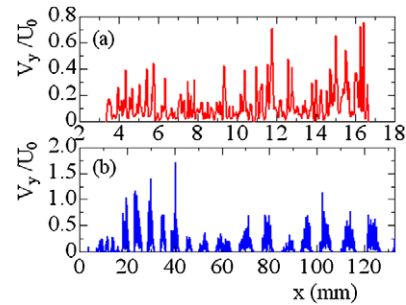

Fig. 4. Profiles of velocity passing through porous wall for $e = 0.6$, $d = 33$ μm; (a) $L = 13$ mm, $U_0 = 10$ cm/s, (b) $L = 133$ mm, $U_0 = 100$ cm/s.

which are typical values of SiC and cordierite filters, respectively [15]. The pore size of 20 μm is also selected between these two values. On the other hand, domain 2 is used for the particle trap simulation. To predict the filter backpressure more precisely, the three-dimensional simulation is needed. This is because the friction factor in the porous media flow is unrealistically higher in the case of two-dimensional calculation [11, 16]. The size of domain 2 is of 0.16 mm × 0.80 mm × 0.16 mm. The total number of grids is 41 (N_x) × 201 (N_y) × 41 (N_z). The inflow velocity, U_0, is 10 and 100 cm/s. In the LB coordinate, non-dimensional variables such as Reynolds number are set to be the same based on the similarity.

As for the boundary condition, the inflow boundary is adopted at the inlet [17]. At the sidewall (top/bottom, front/back), the slip boundary condition is adopted, considering the symmetry [6]. At the outlet, the pressure is constant, and the gradient of soot concentration is set to be zero. On the surface of the diesel filter wall, the so-called bounce-back rule for non-slip wall is adopted [9,11–13].

3. Results and discussion

3.1. Flow in DPF

First, we examine the flow field in DPF. In this section, the flow is simulated without soot accumulation. Fig. 3 shows the velocity field inside the filter. Its porosity is 0.6, and the pore size is 33 μm. The monolith length is 13 mm. In this case, the calculation domain is of 20 mm × 2 mm, and the total number

of grids is 601 (N_x) × 61 (N_y). The distributions of velocity vector, mass flux in the x-direction, and pressure are shown. Since the exit of the monolith is closed, the flow is forced to pass through the porous filter wall, which is well observed in the distribution of the velocity vector in Fig. 3(a). Then, as seen in Fig. 3(b), the mass flux along the filter monolith is gradually decreased. The velocity profile passing through the wall will be discussed later. At the opposite side of the wall, the flow rate is again increased toward the exit. As seen in the pressure distribution in Fig. 3(c), the pressure gradually decreases along the flow path, but there is a huge pressure drop across the filter wall.

Next, the velocity passing through the filter wall is examined. Since the soot particles in exhaust gas are transported by the flow, the particle accumulation is largely affected by the velocity distribution in x-direction (along the monolith). To check the velocity profile using different monolith length, we consider two types of filters of $L = 13$ and 133 mm. To maintain the mean flow velocity across the wall, the inflow velocities for two cases are $U_0 = 10$ and 100 cm/s, respectively. Results are shown in Fig. 4. The porosity and pore size is the same in Fig. 3. It is found that the velocity is smaller than the inflow velocity, because the monolith length is larger than the inlet width (roughly 0.2 mm). In some area, the velocity is almost zero. This is because the flow passes only through the pore inside the filter wall and there are some paths with no exits. Although some variations are observed due to the non-uniformity of the porous structure, the velocity profile is almost uniform along the x-direction.

In order to avoid plugging the filter with diesel particles, we usually monitor the filter backpressure, which depends on the flow velocity, the degree of trapped particles, and the inner structure of the diesel filter. As seen in Fig. 4, independent of the monolith length, the velocity profile is almost uniform along the monolith (x-direction in Fig. 2). Also, the backpressure corresponds to the pressure drop across the filter wall. To reduce the calculation time, only small parts of filter monolith are considered to simulate the flow in domain 2 of three-dimensional calculation. The porous structures of the filter are shown in Fig. 5, which are formed by 3D simulation of two-phase separation [10,12]. The pore sizes of three filters are 9, 20, and 33 μm. The porosity for all cases is 0.42. On the other hand, 2D porous structure needed for Domain 1 is formed by 2D simulation of two-phase separation.
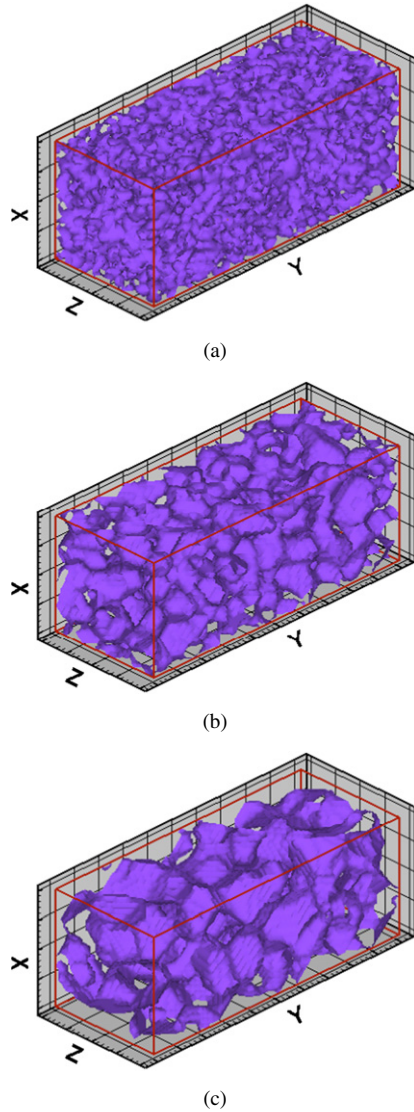
(a)

(b)

(c)

Fig. 5. Porous structure of diesel filter of $e = 0.42$, (a) $d = 9$ μm, (b) $d = 20$ μm, (c) $d = 33$ μm.

Fig. 6. Pressure distributions across filter wall for $d = 9, 20, 33$ μm; $W = 0.4$ mm, $e = 0.42$, $U_0 = 100$ cm/s.

(a) $t = 6$ms

(b) $t = 12$ ms

(c) $t = 30$ ms

Fig. 7. 2D $(x-y$ plane) images of soot accumulation with velocity vector observed in DPF for $e = 0.42$, $W = 0.6$ mm, $d = 33$ μm, $U_0 = 10$ cm/s; (a) $t = 6$ ms, (b) $t = 12$ ms, and (c) $t = 30$ ms.

Here, the pressure is examined inside these different filters. Calculated pressure profiles are shown in Fig. 6. To observe the pressure change in flow direction, the pressure is averaged in $x-z$ plane. The inflow velocity is 100 cm/s, and the filter wall is located at $y = 0.2$ to 0.6 mm. Inside the filter wall, the pressure decreases almost linearly, although it slightly fluctuates for $d = 33$ μm. Outside this region, the pressure is almost constant. To compare three cases, it is found that, as the pore size is smaller, the pressure at the inlet is larger. According to the following Darcy's law,

$$u = -\frac{k}{\mu}\nabla p \qquad (10)$$

where, k is the permeability, μ is the viscosity, and ∇p is the pressure gradient in the flow direction of u. The estimated permeability is 3.2×10^{-13} m^2 for $d = 9$ μm, which is close to 3.7×10^{-13} m^2 of the reported value of SiC DPF [15]. Then, it is confirmed that the porous structure formed by our simulation is similar to the real DPF.
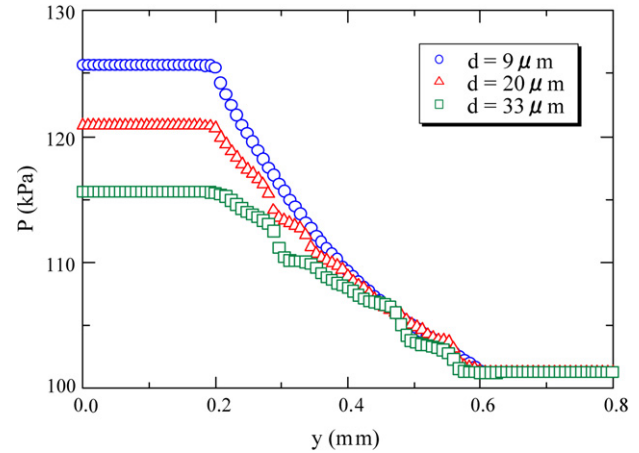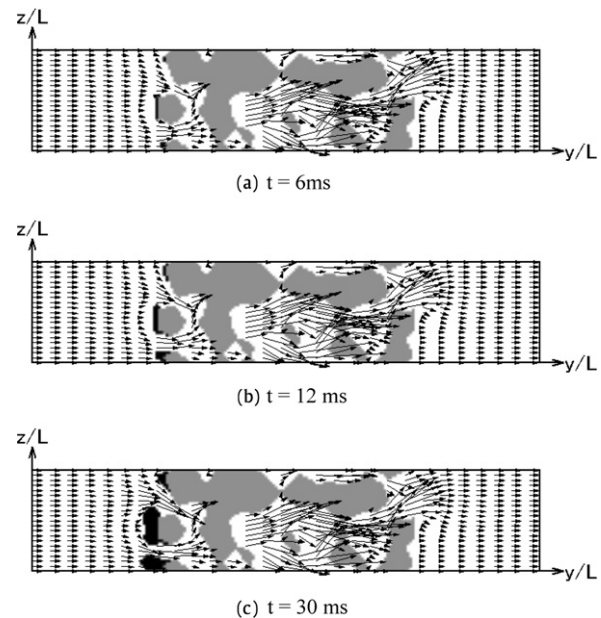
3.2. Soot accumulation

Next, we simulate the soot accumulation. Fig. 7 shows the profiles of accumulated soot in Domain 2. The porosity is 0.42, pore size is 33 μm, and $W = 0.6$ mm, which are the typical values of a cordierite diesel filter. The inflow velocity is 10 cm/s. To precede the soot accumulation in a short time, the soot concentration in exhaust gas is set to be relatively high. The mass fraction of soot at the inlet, $Y_{C,\text{in}}$, is 0.01. The profiles of accumulated soot are shown when the time is 6, 12, and 30 ms, respectively. The black region is the layer of soot deposition, and the gray region is the filter substrate. Only 2D images of $y-z$ plane at center of the calculation domain are shown. When the soot is attached to the filter wall surface, the velocity field is changed due to the smaller porosity. That is, the velocity is largely accelerated at the narrow path due to soot accumulation.
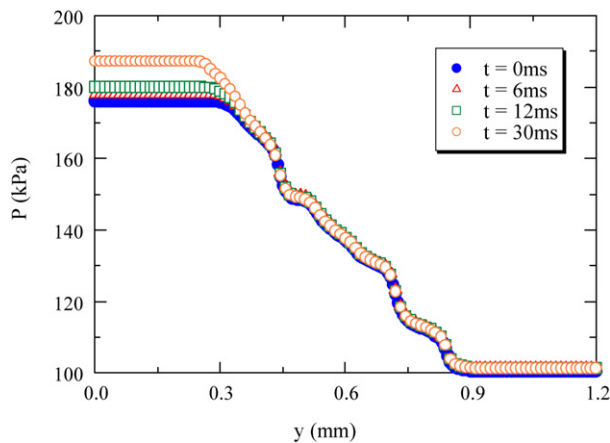
Fig. 8. Pressure distributions with soot accumulation in DPF at $t = 0, 6, 12, 30$ ms; $e = 0.42$, $W = 0.6$ mm, $d = 33$ μm, $U_0 = 10$ cm/s.

The soot is preferably accumulated upstream, which is similar to the observation in experiments [18].

Here, we examine the pressure change with soot accumulation, quantitatively. Fig. 8 shows the pressure distributions. These are the profiles at the time steps of 6, 12, 30 ms, respectively. For comparison, the pressure before the soot accumulation is shown by the profile at $t = 0$ ms. The pressure at the inlet becomes larger as the soot deposition proceeds. That is, the filter backpressure is increased. The similar pressure change is observed when the soot deposited layer is developed in the gas–particle flow [8].

In theoretical consideration, the pressure drop is determined by the trapped soot inside the filter [19]. As more soot is accumulated, the pressure drop is increased. In our simulation, mass of accumulated soot is directly calculated, which is difficult to measure in experiments. More numerical experiments over a wide range of filter properties can be conducted easily, and our approach is very effective to find optimal conditions and construct the better after-treatment of exhaust gas.

4. Conclusions

We have simulated the flow in a wall-flow DPF using the lattice Boltzmann method. The soot accumulation for PM trap has been considered with filters of different length, porosity, and pore size. Results show that, the flow along the filter monolith is uniform, and the large pressure drop across the filter wall is observed, corresponding to the filter backpressure. When the pore size is set to be 9 μm, the estimated permeability based on the Darcy's law is close to the reported value of SiC DPF. In the simulation of soot accumulation, it is observed that the flow pattern is largely changed due to smaller porosity. As the soot concentration inside the filter is increased, the filter backpressure is increased. These are useful information to develop the future diesel filter system.

References

[1] R.A. Searles, D. Bosteels, C.H. Such, A.J. Nicol, J.D. Andersson, C.A. Jemma, Investigation of the feasibility of achieving Euro V heavy-duty emissions limits with advanced emission control systems, in: F02E310, FISITA 2002 World Congress, 2002, pp. 1–17.

[2] G. McNamara, G. Zanetti, Use of the Boltzmann equation to simulate lattice-gas automata, Phys. Rev. Lett. 61 (1988) 2332–2335.

[3] S. Succi, E. Foti, F. Higuera, Three-dimensional flows in complex geometries with the lattice Boltzmann method, Europhys. Lett. 10 (1989) 433–438.

[4] A. Cancelliere, C. Chang, E. Foti, D.H. Rothman, S. Succi, The permeability of a random medium: Comparison of simulation with theory, Phys. Fluids A 2 (1990) 2085–2088.

[5] Y.H. Qian, D. d'Humières, P. Lallemand, Lattice BGK models for Navier–Stokes equation, Europhys. Lett. 17 (1992) 479–484.

[6] T. Inamuro, M. Yoshino, F. Ogino, Lattice Boltzmann simulation of flows in a three-dimensional porous structure, Int. J. Numer. Meth. Fluids 29 (1999) 737–748.

[7] J. Bernsdorf, G. Brenner, F. Durst, Numerical analysis of the pressure drop in porous media flow with lattice Boltzmann (BGK) automata, Comput. Phys. Comm. 129 (2000) 247–255.

[8] O. Filippova, D. Hänel, Lattice-Boltzmann simulation of gas-particle flow in filters, Comp. Fluids 26 (1997) 697–712.

[9] K. Yamamoto, F. Ochi, Soot accumulation and combustion in porous media, J. Energy Inst. 79 (2006) 195–199.

[10] K. Yamamoto, S. Satake, H. Yamashita, N. Takada, M. Misawa, Lattice Boltzmann simulation on porous structure and soot accumulation, Math. Comp. Sim. 72 (2006) 257–263.

[11] K. Yamamoto, N. Takada, M. Misawa, Combustion simulation with lattice Boltzmann method in a three-dimensional porous structure, Proc. Comb. Inst. 30 (2005) 1509–1515.

[12] K. Yamamoto, N. Takada, LB simulation on soot combustion in porous media, Physica A 362 (2006) 111–117.

[13] S. Chen, G.D. Doolen, Lattice Boltzmann method for fluid flows, Annu. Rev. Fluid Mech. 30 (1998) 329–364.

[14] Y.H. Qian, D. d'Humières, P. Lallemand, Lattice BGK models for Navier–Stokes equation, Europhys. Lett. 17 (1992) 479–484.

[15] G.A. Stratakis, A.M. Stamatelos, Flow maldistribution measurements in wall-flow diesel filters, Proc. Instn. Mech. Engrg. 218 (Part D) (2004) 995–1009.

[16] R.B. Bird, W.E. Stewart, E.N. Lightfoot, Transport Phenomena, Wiley, New York, 1960.

[17] X. He, S. Chen, G.D. Doolen, A Novel thermal model for the lattice Boltzmann method in incompressible limit, J. Comput. Phys. 146 (1998) 282–300.

[18] K. Hanamura, T. Tanaka, Visualization study of heterogeneous reaction of particulate matter in regeneration of DPF, in: Proc. JSAE Annual Congress, 20055487, 2005, pp. 23–26.

[19] G.A. Stratakis, D.L. Psarianos, A.M. Stamatelos, Experimental investigation of the pressure drop in porous ceramic diesel particulate filters, Proc. Instn. Mech. Engrg. 216 (Part D) (2002) 773–784.